Paper published in
2024 Supercond. Sci. Technol. 37 065008
DOI 10.1088/1361-6668/ad44e7

Improving the screening ability of high-temperature superconductors by combining disk-shaped bulks and closed-loop coated conductors

N. Rotheudt[1], S. Brialmont[1], J.-F. Fagnard[1], T. Hlasek[2,3], J. Plechacek[2] and P. Vanderbemden[1]

[1] Department of Electrical Engineering and Computer Science, Montefiore Institute B28, University of Liège, B-4000 Liège, Belgium.

[2] CAN SUPERCONDUCTORS, s.r.o., Ringhofferova 66, 251 68 Kamenice, Czech Republic

[3] Department of Inorganic Chemistry, University of Chemistry and Technology Prague, Technická 5, 166 28 Prague 6, Czech Republic

E-mail: nicolas.rotheudt@uliege.be

April 2024

Abstract. In this work, we demonstrate experimentally the remarkable DC magnetic screening ability of hybrid superconducting screens. The configurations under investigation combine a 30 mm-diameter disk-shaped superconducting bulk, or another with a 10 mm-diameter hole, with different closed superconducting loops made from coated conductors. The loops are placed coaxially with the bulk. The bulk superconductors and the closed-loop coated conductors are made of $GdBa_2Cu_3O_7$ and the experiments are performed in liquid nitrogen (77 K). The DC and inhomogeneous field to be screened is produced by a bespoke coil and reaches around 100 mT at the location of the superconducting bulk, which is much less than its full-penetration field. By mapping the magnitude of the flux density using a 3-axis cryogenic Hall probe, we show that such a hybrid superconducting screen allows the maximum shielding factor SF above the bulk to be almost doubled. For the best investigated hybrid configuration, the SF reaches $\sim$ 45 at 2.7 mm above the bulk. In addition, the area of the spatial region for which less than half of the applied field remains (SF $>$ 2) is roughly multiplied by 4 when compared to a situation involving only a disk-shaped bulk. In this work, this region corresponds to a 60 mm-diameter circle. The choice of the loop diameter is found to result from a trade-off between maximum SF and extension of the screened region. Finally, we detail why these hybrid configurations bring such improvements: the key point is that the flux lines generated by the source coil are diverted by the bulk towards a region where the closed-loop coated conductors can oppose the best to them.

1. Introduction

Shielding or screening low frequency stray magnetic fields of possibly large amplitude is required for a wide range of engineering applications. These include high-power density rotating electric machines using superconductors [1–5], magnetic resonance imaging (MRI) magnets [6, 7], current transformers [8], space applications [9] or particle accelerators [10–13]. Conventional ferromagnetic shields are intrinsically limited by their saturation magnetization, e.g. $\mu_0 M_{\mathrm{sat}} \approx 0.7$ T for mu-metal [14]. Superconducting shields do not have such limitations and offer naturally low-frequency 'passive' shielding [15]. The related magnetic shielding mechanism relies on the appearance of induced lossless current loops within the material [16, 17]. By contrast with ferromagnetic shields, the shielding behaviour of superconductors is therefore more sensitive to the geometry of the shield, e.g. the length scale on which the induced currents appear or the presence of gaps [16,18].

High-temperature superconductors (HTS) allow the shield to be operated well above the liquid helium temperature. Two categories of materials are currently used: bulk superconductors and second generation (2G) coated conductors.

Bulk superconductors allow for efficient magnetic shielding well beyond the performances of conventional materials. Several materials can be used in the bulk form, including MgB_2 [19–24], $Bi_2Sr_2CaCu_2O_8$ [25], $Bi_2Sr_2Ca_2Cu_3O_{10}$ [26] and bulk large grain $(RE)Ba_2Cu_3O_7$ where (RE) denotes a rare earth [27–30]. Both MgB_2 [24] and Bi-based materials can be processed in long tubes. Growing large bulk HTS plates, however, remains a challenge and the screening of stray magnetic fields using planar bulk superconductors is often limited to a few cm^2. One possible solution is to arrange side-by-side several bulks. Such a topology may require several layers of bulks in a brick-wall arrangement to mitigate the presence of gaps between them [18, 31–33].

On the other hand, HTS coated conductors can be processed over long lengths. Two methods can be used to shield a magnetic field using coated conductors. The first method involves using arrangements made of several tapes. These can be made of short segments of coated conductor juxtaposed, stacked above one another [34–37] or arranged as a paraboloid [38]. They can also be placed along the axis of a cylindrical former [39, 40], wound around the former as a solenoid [34, 39–43] or arranged as rings [34, 44], possibly combined with active shielding [45]. These tapes can be used to reduce the amplitude of an external field or to improve the homogeneity of the field component parallel to them [46, 47]. Stacked tape annuli can also be created [48] and were recently shown to shield up to 0.67 T at 77 K [49]. The second method is to use coated conductors as naturally short-circuited 'eye-shaped' loops in which persistent currents are induced [50, 51]. Importantly, such loops are easily scalable, which may require to adapt its geometry [52], and offer the opportunity to screen the stray field of any electric device of large size. Another advantage of these closed-loop coated conductors is the absence of resistive soldering, allowing therefore quasi-static fields to be shielded.

In very few cases, the properties of magnetic shields combining bulk and soldered tapes were also explored [53]. Since bulks and coated conductors have distinct advantages (efficient magnetic shielding for the bulks and scalability for the coated conductors), their combination may be very useful to consider. However, a systematic study of the benefits brought by bulk superconducting disks and closed-loop coated conductors is lacking.

The purpose of the present work is to demonstrate experimentally how hybrid superconducting configurations, i.e., combining both disk-shaped bulks and closed-loop coated conductors, can be used to improve significantly the DC or quasi-static screening ability of either bulks or coated conductors. This paper is organised as follows. In section 2, we first describe the experimental process and the different studied configurations. Section 3 deals with the experimental results. In section 3.1, we compare the magnetic screening performance of hybrid screens to those achieved using only bulks or tapes. In section 3.2, we study different hybrid configurations and discuss how the size of the superconducting closed loops can be chosen the most efficiently. Finally, in section 4, we discuss in more details the shape of the flux lines diverted by several hybrid configurations in order to understand intuitively the spatial distribution of the flux density behind the screen.

2. Experimental set-up

The geometry of the experiments is shown schematically in Figure 1. A source coil generates an inhomogeneous DC field. The superconducting screen is placed above the coil. The supercurrent loops induced in the superconducting parts oppose the field generated by the source coil. The flux density is measured in the region above the superconducting screen.

Based on this geometry, we studied 11 different superconducting screens, using three types of samples: a disk-shaped bulk, a hollow (ring-shaped) bulk and several closed-loop coated conductors. These 11 different configurations are shown schematically in Figure 2. The bulks used in this study are single-

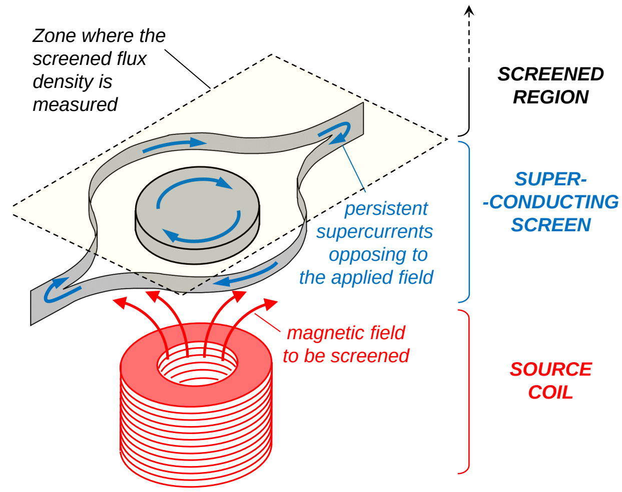

Figure 1. Schematic illustration of the experiments carried out in this work.

domain melt-textured GdBCO/Ag ($GdBa_2Cu_3O_7$ + 0.4 mol Gd_2BaCuO_5 + 10% Ag_2O) samples produced by the novel 'single-direction melt growth' (SDMG) method [54, 55] at Can Superconductors, s.r.o. The details of the synthesis process are described in [56]. Both the disk-shaped bulk and the hollow bulk have a thickness of 5 mm, an outer diameter of 30 mm and a uniform critical current density J_c around 2 10^8 A/m^2 at T = 77 K. The hollow sample features a 10 mm-diameter hole. The closed-loop coated conductors are obtained from a 10 mm-wide second generation (2G) GdBCO tape from Shanghai Superconductor. The critical current of the coated conductor is of the order of 500 A at 77 K and self-field. The loop is created by milling a slit in the middle of a coated conductor segment to form a closed superconducting loop, allowing persistent currents to flow [50,51,57–62]. Both parts of the coated conductor can therefore be extended around a cylindrical holder. In the following, we will call 'diameter of the loop' the diameter of the underlying cylindrical holder. In order to increase the equivalent total supercurrent that can flow in the loop, four similar closed-loop coated conductors are superimposed on four layers.

The superconductors are placed on a 3D-printed PA6CF (from Polymaker) sample holder as shown in Figure 3**(a)** for the configuration combining the disk-shaped bulk with 45 mm- and 60 mm-diameter closed-loop coated conductors (denoted by 'B + 45 mm-⊘ L + 60 mm-⊘ L' in Figure 2). The bulk sample is placed in a hole in the sample holder and is secured in place with a Kapton® sheet to prevent it from moving during the experiment. The loops are centred around the bulk sample. It is worth mentioning that the height of the top surface of the bulk, corresponding

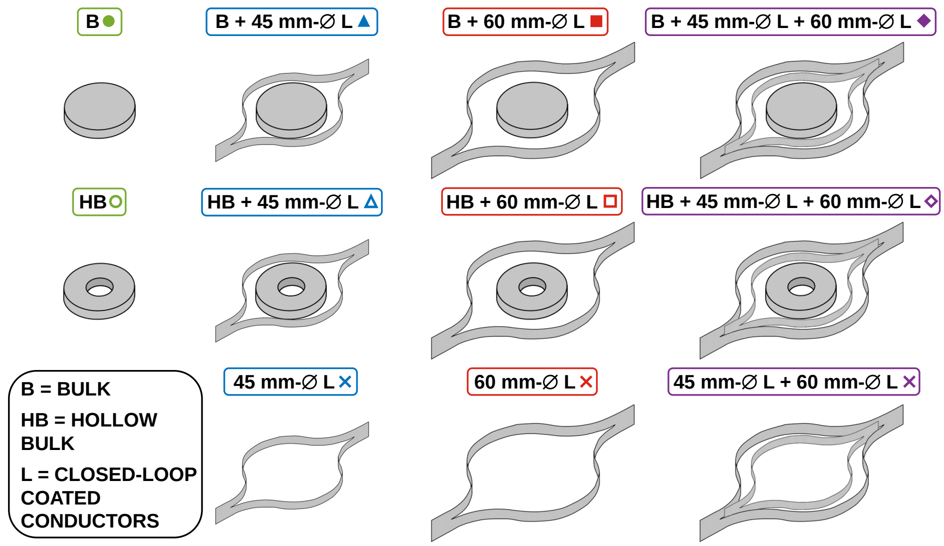

Figure 2. Schematic drawing of the different configurations studied in this work. B stands for disk-shaped bulk, HB for hollow bulk, L for closed-loop coated conductors and ∅ for diameter. The symbols associated to each configuration are those used in the following figures.

to $z = 0$ in the following, is exactly that of the slit of the loops. The direction of the x and y axes are also shown in Figure 3**(a)**. This 3D-printed sample holder is fixed on a PVC structure made of two parallel plates. The source coil generating the inhomogeneous magnetic field to be screened is placed between these plates. The source coil is centred with respect to the bulk, as shown in Figure 3**(b)**. This coil is made of 4300 turns of 0.3 mm-diameter copper wire wound along a height of 33 mm. The outer diameter of this coil is around 46 mm. Its electrical resistance is around 100 Ω at room temperature and 12 Ω at 77 K. In order to increase the applied magnetic field in the region close to the axis of the coil, a ferrimagnetic core is inserted in the coil bore. This core is a MnZn ferrite rod having a height of 41.3 mm and a diameter of 12.3 mm. The ferrimagnetic core is placed such that its top surface is almost in contact (spacing of ~ 0.2 mm) with the bottom surface of the bulk (i.e., $z = -5$ mm). In order to monitor the temperature at the centre of the coil during the current injection and prevent local heating, a type T (copper-constantan) thermocouple was inserted inside the coil at the beginning of the winding process. With this set-up, the goal is therefore to screen the region $z > 0$ from the inhomogeneous field produced by the source coil.

The inhomogeneous flux density produced by the source coil in the absence of superconducting screen was measured to characterise its main features. For measuring simultaneously the distribution of the three components of $\vec{B}$, we use a bespoke 3-axis cryogenic Hall probe that we designed in a previous work [63] attached to a xyz micro-displacement system. The xyz displacement system consists of three independent motorised stages able to move the Hall probe in a volume of 300 mm × 300 mm × 200 mm (OSMS33-300(XY) and OSMS26-200(Z); Optosigma).

To design the 3-axis cryogenic Hall probe, we took advantage of a commercially available room-temperature 3-axis Hall sensor (MLX90395; Melexis) placed inside a thin cylindrical insert whose inner temperature is carefully controlled to be 25 ± 0.2°C, irrespective of the outer cryogenic temperature (77 K). This temperature control is managed by a dedicated interfacing electronics placed close to the Hall sensor. In this system, the active area (here equivalent to a 250 µm-radius circle) of the Hall sensor is located at 2.2 ± 0.25 mm from the bottom of the insert, which sets the minimal height $z_{\rm min}$ that can be mapped in our experiments. The typical uncertainty associated with the measurements is around 100 µT.

Figure 3**(c)** shows the flux lines drawn from the measurement of $\mu_0\vec{H}_{\rm app}$ generated by the source coil in the plane $x = 0$. The component parallel to z is therefore the axial component and that parallel to y is the radial component. The background colour shows the magnitude of the local magnetic flux density measured when the source is fed with 0.5 A, which is the maximum allowed current. The generated flux density is around 52 mT at the location $(x, y, z) = (0, 0, 0)$. Figure 3**(c)** illustrates how the inhomogeneous source field is deflected with respect to the main (axial) direction. For example, at

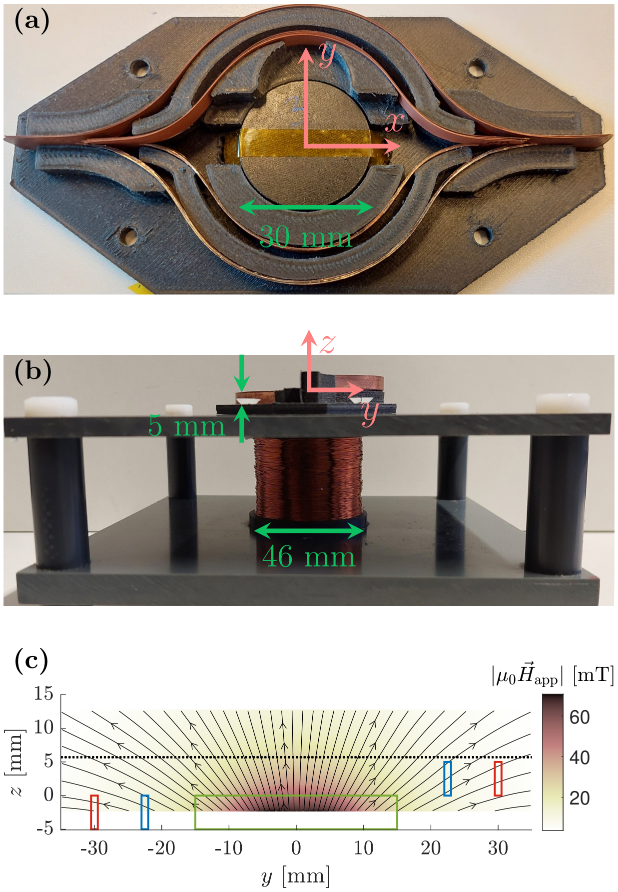

Figure 3. (a) 3D-printed sample holder with the superconducting samples corresponding to the configuration B + 45 mm-⊘ L + 60 mm-⊘ L. **(b)** Front view of the experimental set-up consisting of the sample holder and the source of inhomogeneous magnetic field (coil with ferrite) placed between two parallel PVC plates. The spatial region to be screened corresponds to $z > 0$. **(c)** Flux lines drawn from the measurement of $\mu_0\vec{H}$app generated by the source coil in the plane $x = 0$. The background colour shows $|\mu_0\vec{H}$app$|$. The green rectangle shows schematically the position of the bulk in the experiments. The blue (resp. red) rectangles indicate the cross-section of the 45 mm-diameter (resp. 60 mm) closed-loop coated conductors. The black dotted line corresponds to $z = 5.7$ mm.

$(x, y, z) = (0, 30, 5.7)$ mm, i.e., right above the 60 mm-diameter loops, at a typical height where magnetic measurements will be carried out in the following, the flux density is deflected by approximately 64° from the z-axis. It can also be noted that the z component is positive for the whole considered region, i.e., the superconducting screen is placed in a region where there are no 'return lines' of the source field.

For each of the 11 configurations, as well as for the source coil alone, i.e., without superconducting screen, we carry out the experiment described by the following process:

(i) Cool the entire structure down to 77 K (liquid nitrogen) without applied field. Wait for the liquid nitrogen bath to stop boiling and for the thermocouple temperature to be stable.

(ii) Apply a DC current I in the coil. Initially, $I = 0.1$ A.

(iii) Wait for 5 minutes. The purpose of this step is to ensure that the results are almost independent of time-dependent physical phenomena related to flux creep.

(iv) Simultaneously measure the spatial evolution of B_x, B_y and B_z along y, for $x = 0$, at four different values of $z > 0$, using the set-up described above, i.e., a combination of an xyz micro-displacement system and a bespoke 3-axis cryogenic Hall probe.

(v) Repeat the previous step once to check the repeatability of the measurements.

(vi) Exactly 30 min after step (ii), repeat steps (ii) to (vi) with I increasing to $I + 0.1$ A. Stop after reaching 0.5 A.

3. Results

We show here the experimental results obtained with the set-up described in section 2 for particular configurations selected to illustrate the main differences between them. The results for the configurations that are not shown in this section are available in Appendix A.

Two metrics are used to illustrate the experimental results. First, we show the magnitude of the flux density $|\vec{B}| = \sqrt{B_x^2 + B_y^2 + B_z^2}$ computed from the components measured by the Hall probe. We compare this with $|\mu_0\vec{H}_{\rm app}|$, the applied field measured in the absence of superconducting screen. Second, we characterise the local screening efficiency of a given configuration by the shielding factor SF, defined as

$$\mathrm{SF} = \frac{\left|\mu_0\vec{H}_{app}\right|}{\left|\vec{B}\right|}. \quad (1)$$

From this definition, the larger the SF, the most efficient the screening.

Following the measurement sequence outlined in section 2, the initial observation is that, within experimental uncertainty, no perceptible difference is found between the two similar mappings for a specific configuration at a given applied field, i.e., between steps (iv) and (v) as described in section 2. This result gives confidence in the repeatability of the measurements and strongly suggests that they are not affected by time-dependent phenomena. Hence, only the results from the second set of mappings (step (v)) are presented in the following.

The second point common to all measurements shown below is that, even with the maximum applied field, the superconducting bulks are very weakly penetrated. This is because the local field is much less than their full-penetration field. It means that the magnetic flux lines that can reach the region $z > 0$ are mainly those going *around* the bulk sample. More details about the shape of the magnetic flux lines are given in section 4. Additionally, the current that flows in the closed-loop coated conductors is much smaller than the critical current. Hence, when the applied field increases, the flux embraced by the loop increases and the current in the loop increases. The practical implication of these observations (neither the bulk nor the loops being fully penetrated) is that the shielding factor SF is found to be independent of the value of the applied field, within experimental uncertainty. Consequently, only the results for the largest applied field, i.e., with 0.5 A in the coil, are considered in the following.

3.1. Interest of hybrid configurations

In the geometry considered here and illustrated in Figure 1, a superconducting bulk can provide a very efficient screening effect right above its centre, not too far from the surface. However, this screening will be strongly limited by the flux lines going around the bulk. This effect cannot be reduced as the diameter of large grain, bulk (RE)BCO materials cannot be scaled up easily. On the opposite, the closed-loop coated conductors can be scaled up significantly. In the case of large loops, however, the supercurrent flowing in the loops provides a rather small magnetic field in the central region of the loops, hence a very limited screening effect in this region. This relates to the fact that, for a given current in the loop, the field B_c induced at the centre of the loop decreases as the diameter of the loop D increases, approximately following the relationship $B_\mathrm{c} \sim 1/D$.

Figure 4 compares the screening properties of a bulk alone, closed-loop coated conductors alone, and both combined together (hybrid configuration). Figure 4**(a)** shows the spatial distribution of the magnitude $|\vec{B}|$ of the magnetic flux density along y, for $z = 5.7$ mm and for the maximum applied field. Due to the offset between the two legs of the closed-loop coated conductors, measurement points can only be taken for $y < 12$ mm with our experimental system.

The first observation is that the distribution of the field produced by the source coil is bell-shaped and symmetrical around $y = 0$, as expected. The presence of the bulk reduces significantly the magnitude of

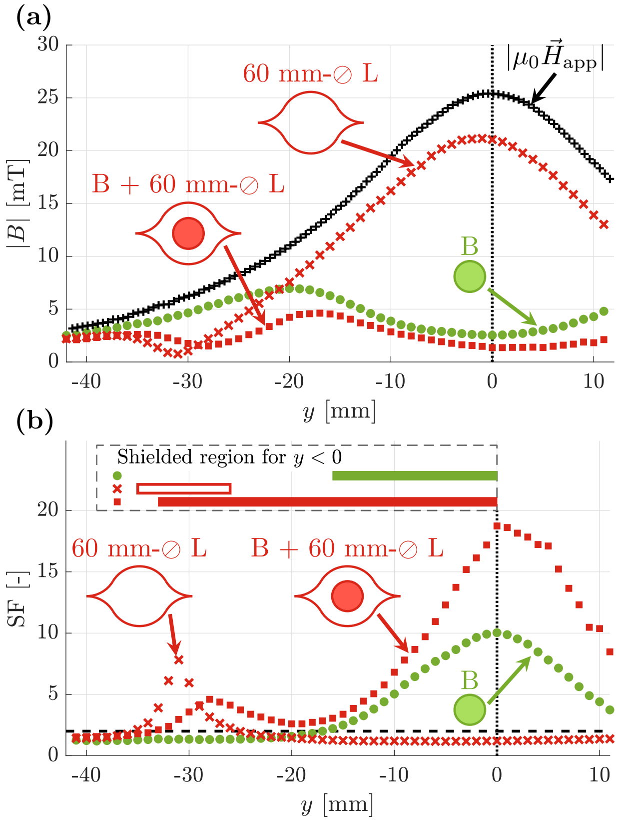

Figure 4. **(a)** Spatial distribution of the magnitude $|\vec{B}|$ of the magnetic flux density along y, for $z = 5.7$ mm and for the maximum applied field. The applied field in the absence of superconducting screen is shown with black plus symbols **+**. The solid green circles ● show the flux density when the 30 mm-diameter disk-shaped bulk is used as a screen. The red crosses **×** depict the situation with the 60 mm-diameter closed-loop coated conductors alone. The solid red squares ■ correspond to the hybrid configuration, combining the bulk and the loops. The dotted black line indicates the central position $y = 0$. **(b)** Spatial distribution of the shielding factor SF along y, for $z = 5.7$ mm. The coloured symbols are the same as in **(a)**. The rectangles at the top of the graph indicate in each of the three cases the spatial extension of the region SF > 2 for $y < 0$. The limit SF $= 2$ is shown by a dashed black line.

the flux density above the centre. However, for $|y| > 15$ mm (15 mm being the radius of the bulk), the measured flux density increases and progressively tends to reach the flux density measured with no bulk. On the opposite, for the closed-loop coated conductors alone, the flux density above the centre is poorly attenuated. The flux attenuation is much better around $|y| = 30$ mm, i.e., right above the coated conductors. When combining the bulk with the loops to obtain a hybrid configuration, the advantages of both configurations are kept, yielding a significant magnetic flux attenuation over an extended range.

Figure 4**(b)** presents the exact same data as Figure 4**(a)** but in a way which is better suited to investigate the screening properties. Figure 4**(b)** shows the spatial distribution of SF along y, for $z = 5.7$ mm. For the bulk alone, the SF reaches 10 above its centre and the closed-loop coated conductors alone have a SF around 1.2 at the same position. Significantly, when both of them are combined (hybrid configuration), the SF above the centre reaches 18.7, i.e., it is almost doubled with respect to the bulk alone and multiplied by a factor greater than 15 compared to the loops alone. Figure 4**(b)** also shows that the spatial extension of the screened region increases considerably with the hybrid configuration. In order to illustrate this, the rectangles at the top of Figure 4**(b)** represent, for $y < 0$, the spatial extension of the region SF > 2, i.e., for which the measured field is $<$ 50% of the applied field. The spatial extension of the region SF > 2 is $|y| \lesssim 16$ mm for the bulk alone (roughly the size of the bulk) and only a small region around $y = 30$ mm for the closed-loop coated conductors. For the hybrid configuration, this region extends up to $|y| \approx 33$ mm, i.e., twice further than for the bulk alone. Importantly, this corresponds to a screened surface ~ 4 times larger.

This set of results gives evidence that considering hybrid configurations is very beneficial for magnetic screening. Compared to what can be achieved with a bulk alone, the maximum SF is increased almost by a factor 2 and the surface of the screened region is extended by a factor ~ 4.

3.2. Comparison between different hybrid configurations

The previous section has shown that adding closed-loop coated conductors to a disk-shaped bulk can considerably improve its screening performance. As these loops can be scaled up very easily, the natural question that arises is how large the size of the loops should be chosen. To provide elements for addressing this question, three configurations are compared in this section: the disk-shaped bulk is combined either with 45 mm-diameter loops or with 60 mm-diameter loops or with both 45 mm- and 60 mm-diameter loops.

Figure 5 shows the spatial distribution of SF along y, for $z = 5.7$ mm. The first observation is that the maximum SF is smaller for 60 mm-diameter closed-loop coated conductors than for 45 mm. This relates to the fact that the larger the loop, the smaller the field that can be generated around its centre (with the same current) to oppose the applied field. Combining both sizes of loops allows us to reach a globally higher SF, as expected intuitively. The second observation relates to the spatial extension of the screened region. The results show that when only one loop diameter is used, this spatial extension is roughly as large as the considered loop. When considering loop diameters

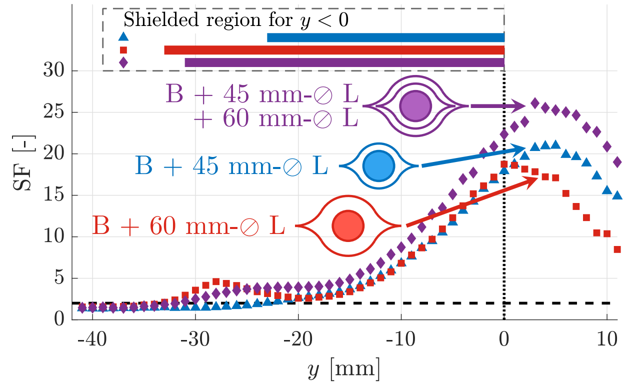

Figure 5. Spatial distribution of SF along y, for $z = 5.7$ mm. The solid blue triangles ▲ show the SF when the bulk is combined with 45 mm-diameter closed-loop coated conductors. The solid red squares ■ depict the situation with the bulk combined with the 60 mm-diameter loops. The solid violet diamonds ◆ correspond to the bulk with 45 mm-diameter loops and 60 mm-diameter loops. The dotted black line indicates the central position $y = 0$. The rectangles at the top of the graph indicate in each of the three cases the spatial extension of the region SF > 2 for $y < 0$. The limit SF $=$ 2 is shown by a dashed black line.

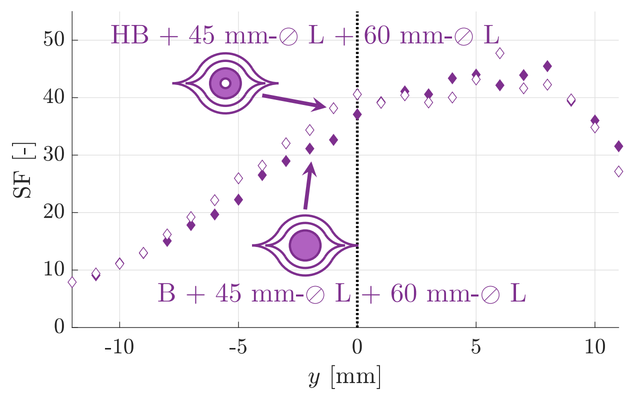

Figure 6. Spatial distribution of SF along y, for $z = 2.7$ mm. The solid violet diamonds ◆ show the SF when the full disk-shaped bulk is combined with 45 mm-diameter and 60 mm-diameter closed-loop coated conductors. The open violet diamonds ◇ depict the situation when the hollow bulk is combined with the 45 mm- and 60 mm-diameter loops. The dotted black line indicates the central position $y = 0$.

up to twice the diameter of the disk-shaped bulk, there is therefore a clear trade-off in the choice of the size of the closed-loop coated conductors. Choosing a small diameter increases slightly the maximum SF while choosing a large diameter increases the spatial extension of the screened region. If the application allows it, the best solution is to combine loops of increasing size, which guarantees an efficient screening effect over a large region.

Since the best screen among the three investigated configurations is that combining the 45 mm- and 60 mm-diameter loops, it is interesting to investigate the maximum SF that it can provide and whether a hole at the centre of the bulk has any visible influence on the magnetic screening properties. Figure 6 shows the spatial distribution of SF along y, but this time, closer to the screen ($z = 2.7$ mm), in order to reach higher SF values. The main observations are the following. First, the SF that can be reached is as high as ~ 45. Second, for the maximum applied field considered here and 2.7 mm above the bulk surface, no significant influence of the 10 mm-diameter hole can be seen.

4. Discussion

In order to understand why the hybrid configurations bring such significant improvements in the superconducting screening abilities, it is helpful to consider the qualitative behaviour of the flux density lines. Figure 7 shows schematically part of the flux lines in two different cases, as a cross-section in the plane $x = 0$. On the left, the inhomogeneous field produced by the source coil is shown. When considering the loops alone, the field they are subjected to in this case has an important radial component and, importantly, is much larger at the centre than close to the superconductor itself. When screening supercurrents are induced in these loops, the field generated by these supercurrents to oppose the applied field in the plane of the slit (or at small z) is rather small at the centre, and maximum close to the superconductor. In this situation, the closed-loop coated conductors intended for magnetic screening are thus used *inadequately* since the spatial distribution of the field generated by these induced supercurrents differs strongly from the spatial distribution of the applied field. This phenomenon was shown in Figure 4 for the 60 mm-diameter loops: the field attenuation is found to be low (except above the superconductor) because of these differences in the magnetic field distribution. The results for the 45 mm-diameter loops are shown in Appendix A.

On the right side of Figure 7, the influence of the disk-shaped bulk on the flux lines distribution is illustrated. As mentioned before, the flux lines are expected to penetrate the bulk sample over a characteristic length d much smaller than the geometric dimensions of the sample. With our set-up, $J_c \approx 2\ 10^8$ A/m^2 and the field amplitude at the bottom surface of the bulk, i.e., at $(x, y, z) = (0, 0, -5)$ mm, is $\mu_0 H_{app} \approx$ 100 mT. Hence, a rough estimate of the characteristic length is $d \sim H_{app}/J_c \approx 0.4$ mm, which is much smaller than the bulk thickness (5 mm). In a first approximation, it is fair to assume that the bulk is almost not penetrated. Hence, the largest part of the flux lines bends around the bulk, their local concentration increases around the bottom surface and the lateral edge of the disk-shaped bulk, and supercurrents are induced only in a small part of the superconductor,

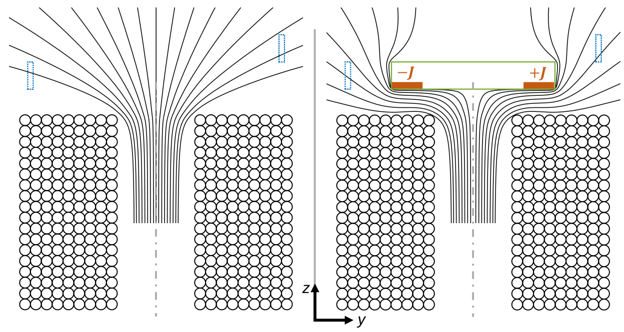

Figure 7. Schematic representation (cross-section) of the flux lines in two different cases: without superconducting screen (left) and with a disk-shaped bulk (right). In both cases, the position of 45 mm-diameter closed-loop coated conductors is shown in blue. The induced currents are indicated in brown.

as shown schematically in brown in Figure 7. This distorted shape of the flux lines caused by the presence of the bulk sample is the key point to understand why the hybrid configurations bring the improvements shown in the results above. When adding the closed-loop coated conductors (dotted blue rectangles) around the bulk, the flux lines embraced by these loops have a totally different shape compared to the situation where the screen consists of the superconducting closed-loop coated conductors alone. In hybrid configurations, the flux lines are mainly parallel to the surface of the loops and, importantly, are located close to the surface of the coated conductors. Therefore, the loops are used in an *optimal* way: the lines of applied field to be screened are forced to meander close to the coated conductor loops, exactly where the induced currents in these loops can produce the largest opposite field. This explains intuitively why these hybrid configurations have screening abilities that largely surpass those of bulks alone or of loops alone.

It is important to highlight that the discussion above focuses on local magnetic phenomena, i.e., the local density of flux lines. In practice, the shielding behaviour results from both local and global phenomena. One of these global phenomena is the flux picked up by the loops: the larger the flux, the larger the current induced in the loops and the larger the SF. When a bulk is used in the hybrid screen, flux lines are diverted and the flux picked up by the loops is smaller than when they are used alone. Another advantage of hybrid configurations is therefore the following. If the closed-loop coated conductors are used alone to screen an increasingly large applied field, once the current reaches the critical current, the SF drops. The addition of the bulk helps thus the coated conductors to screen larger fields by reducing the amount of induced current needed to achieve a certain level of shielding. Such an interpretation is not discussed in more details in this paper since the current flowing into the coated conductors is here much smaller than the maximum current, as shown below.

In order to deepen the intuitive explanation about Figure 7, the opposite field induced by each type of superconducting sample used in the hybrid screen can be considered. In the following discussion, we take advantage of using a cryogenic 3-axis Hall probe to be able to consider simultaneously the spatial distribution of B_y and B_z along the y-axis. In the considered geometry, B_y corresponds to the radial component of the flux density and B_z is the axial component.

The distribution of the induced flux density $B_{\mathrm{ind},y}$ and $B_{\mathrm{ind},z}$ along y is shown in Figure 8**(a)** and Figure 8**(b)** respectively. The induced flux density is defined here as the flux distribution generated by a given superconducting screen to cancel out the source field. Hence, it is obtained by subtracting the flux density in the presence of the superconducting screen from the flux density without this screen. The solid green circles correspond to the flux density induced by the bulk, obtained by subtracting the flux density measured when the disk-shaped bulk is used as a screen from the source field. The green line is an analytical estimation of the induced flux density using Biot-Savart's law. It assumes that a current density $J = J_c = 2\,10^8$ A/m^2 flows in the bottom corner of the disk-shaped bulk, as shown schematically in Figure 7. The cross-section of this current distribution is assumed to be a rectangle of height 0.9 mm and width 5.6 mm. These dimensions correspond to typical dimensions for which the analytical estimation reproduces nicely the experimental distribution of induced flux density, keeping the nominal value of J_c. Although this assumed distribution of J_c provides an oversimplified description, Figure 8 illustrates that it reproduces very well the distribution of the induced flux density. This result validates a posteriori the current distribution drawn in Figure 7.

The solid blue triangles correspond to the measurement of the flux density induced by the combination of the disk-shaped bulk and the 45 mm-diameter closed-loop coated conductors used as a screen. The blue line is an analytical estimation of the induced flux density. It is obtained by summing the green line with an estimation of the field produced by the loops using Biot-Savart's law. For this estimation, we assume a uniform current distribution in the coated conductor tape over half its width, i.e., 4.75mm. This latter dimension takes into account that 0.5 mm of tape are removed by the milling process. For calculating the field analytically, this half-width of coated conductor is replaced by a sheet of 10 parallel, equally spaced and infinitely thin wires. The equivalent total current

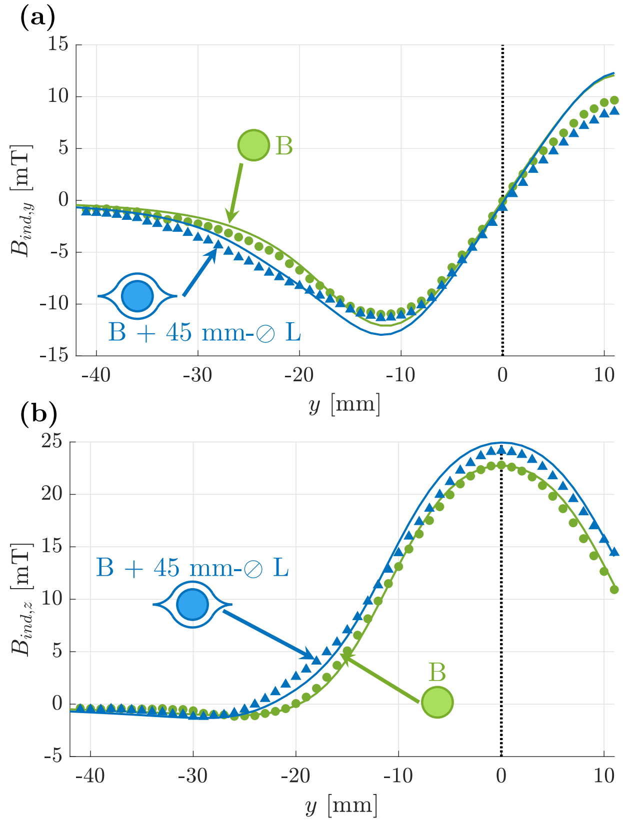

Figure 8. **(a)** Spatial distribution of the induced flux density $B_{\mathrm{ind},y}$ along y, for $z = 5.7$ mm and for the maximum applied field. The solid green circles ● are the measurements of the flux density induced by the disk-shaped bulk when used alone as a screen (difference between applied field and field with the screen). The solid blue triangles ▲ are the measurements of the flux density induced by the combination of the bulk with 45 mm-diameter closed-loop coated conductors used as a screen. The lines are analytical estimations corresponding to both cases and using Biot-Savart's law. The dotted black line indicates the central position $y = 0$. **(b)** The same applies for $B_{\mathrm{ind},z}$.

flowing in the loops is assumed to be 90 A, which is a typical value for which the measurements of the flux density are reproduced quantitatively. It is important to emphasize that such a current is much smaller than the maximum current that can flow in the loops, which validates a posteriori the discussion above. Simply adding the field produced by the coated conductor to the field produced by the bulk sample is a crude approximation since it neglects the magnetic coupling between them. In spite of this simplified approach, the results plotted in Figure 8 show that the main features of the flux density distribution are very well reproduced for both the radial and the axial components of the flux density. Therefore, this intuitive explanation can be used to help understand the magnetic behaviour of these screens and can be extended to other geometries.

If superconducting joints were easily available, a perfectly circular closed loop could be created and

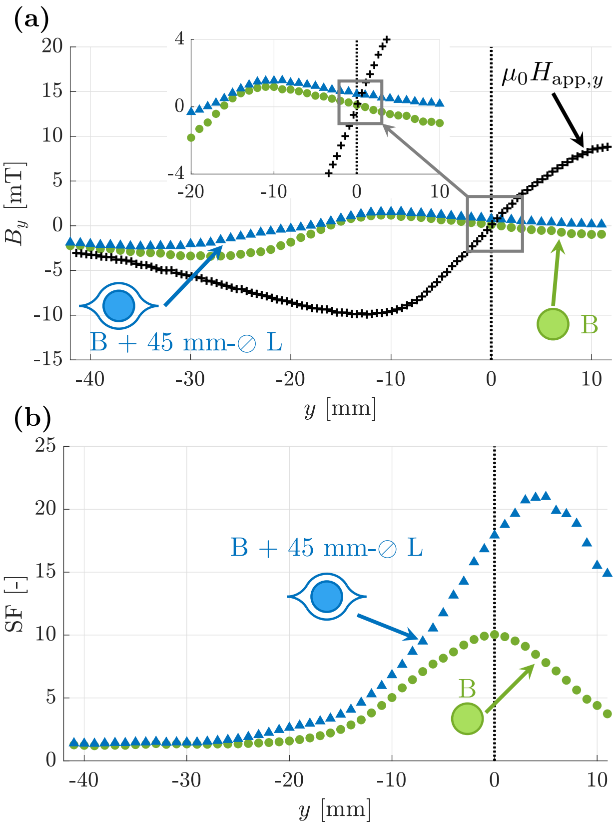

Figure 9. **(a)** Spatial distribution of B_y along y, for $z = 5.7$ mm and for the maximum applied field. The applied field in the absence of superconducting screen is shown with black plus symbols **+**. The solid green circles ● show the flux density when the 30 mm-diameter disk-shaped bulk is added. The solid blue triangles ▲ depict the situation with the hybrid configuration with the bulk and the 45 mm-diameter closed-loop coated conductors. The dotted black line indicates the central position $y = 0$. **(b)** Spatial distribution of the shielding factor SF along y, for $z = 5.7$ mm. The coloured symbols are the same as in **(a)**.

the main previous results and explanations would still hold. However, here, the loops are asymmetric because of the vertical offset between both halves of the loop. This yields interesting features to consider to deepen our understanding of the magnetic shielding process.

Figure 9 compares the same configurations as those discussed in Figure 8. In Figure 9**(a)**, the distribution of B_y along y is shown. The first observation is that the sign of B_y is fully consistent with the qualitative explanations related to Figure 7. Once the bulk is added, the flux lines go around it in such a way that B_y becomes positive between $y \approx -16$ mm and $y = 0$ mm. For $y < -16$ mm and for $0 < y < 12$ mm (measurement range), B_y is negative. The second observation relates to the value of B_y at the centre of the plane, i.e., for $y = 0$. For the applied field or when the disk-shaped bulk is used as a screen, $B_y(y = 0)$ is zero, as can be expected due to the axisymmetry present in these configurations. However, because of the vertical offset between both halves of the closed-loop coated conductors, the axisymmetry is broken: the field generated by the screening supercurrents above the centre has a main component parallel to z but has also a smaller component along y. This explains why $B_y(y = 0) > 0$ (as illustrated in the inset) for the configuration involving the loops.

In addition, when measuring the distribution of $|\vec{B}|$ for the hybrid configurations, the results are not symmetric around $y = 0$. For example, for the configuration described in this section (disk-shaped bulk with 45 mm-diameter loops), $|\vec{B}| \approx 2.9$ mT for $y = -10$ mm and $|\vec{B}| \approx 1.2$ mT for $y = 10$ mm. The main reason is that the measurements are taken at $z = 5.7$ mm and not $z = 0$. Because of the offset between the two halves of the closed-loop coated conductors, the distance to the closest superconducting part for $y > 0$ is smaller than for $y < 0$ (see Figure 3). As a consequence, for $z > 0$, the field generated by the supercurrents induced in the loops for $y > 0$ is larger than that generated for $y < 0$, which results in a higher shielding factor SF for positive values of y. This asymmetry is highlighted in Figure 9**(b)**, which shows the spatial distribution of SF. While the maximum SF is reached for $y = 0$ in the absence of loops, it is reached for $y \approx 5$ mm for the hybrid configuration.

5. Conclusion

In this work, we demonstrated experimentally the remarkable screening efficiency of hybrid configurations combining a disk-shaped or ring-shaped superconducting bulk with closed-loop coated conductors. The experiments were performed at $T = 77$ K, with an inhomogeneous DC applied field around 100 mT at the bottom surface of the bulk, coaxial with the superconducting samples. By mapping the magnitude of the flux density using a 3-axis cryogenic Hall probe, we showed that adding closed-loop coated conductors coaxially to a disk-shaped bulk allows the maximum shielding factor SF above the bulk to be almost doubled. For the optimal configuration combining the bulk with 45 mm- and 60 mm-diameter closed-loop coated conductors, the shielding factor reaches ~ 45 at 2.7 mm above the bulk. In addition, the area of the spatial region for which less than half of the applied field remains (SF > 2) is roughly multiplied by 4 compared to a situation where only a disk-shaped bulk is used. Experimental results showed that the choice of the diameter of the closed-loop coated conductors results from a trade-off: the larger the diameter, the larger the spatial extension of the screened region but the smaller the maximum SF. A diameter of the closed-loop coated conductors of twice the diameter of the bulk sample was found to be an adequate choice to increase significantly the spatial extension of the screened region. The experimental results allowed to explain intuitively why hybrid configurations provide such a significant improvement with respect to the bulk alone: the magnetic field lines generated by the source coil are diverted towards a region where the closed-loop coated conductors can oppose the best to them.

Acknowledgments

This work was supported by the Fonds de la Recherche Scientifique - FNRS under grant CDR n° J.0184.23. Nicolas Rotheudt is recipient of an FRS-FNRS Research Fellow grant.

References

[1] Haran K S, Kalsi S, Arndt T, Karmaker H, Badcock R, Buckley B, Haugan T, Izumi M, Loder D, Bray J W, Masson P and Stautner E W 2017 *Supercond. Sci. Technol.* **30** 123002
[2] Haran K S, Loder D, Deppen T O and Zheng L 2016 *IEEE Trans. Appl. Supercond.* **26** 202508
[3] Song X, Mijatovic N, Kellers J, Bührer C, Rebsdorf A V, Hansen J, Christensen M, Krause J, Pütz H, Wiezoreck J and Holbøll J 2017 *IEEE Trans. Appl. Supercond.* **27** 5201205
[4] Netter D, Leveque J, Ailam E, Douine B, Rezzoug A and Masson P 2005 *IEEE Trans. Appl. Supercond.* **15** 2186–2189
[5] Dorget R, Nouailhetas Q, Colle A, Berger K, Sudo K, Ayat S, Lévêque J, Koblischka M, Sakai N, Oka T and Douine B 2021 *Materials* **14** 2847
[6] Seidel P (ed) 2015 *Applied Superconductivity: Handbook on devices and applications* (Wiley)
[7] Wang Y, Wang Q, Wang H, Chen S, Hu X, Liu Y and Liu F 2021 *Supercond. Sci. Technol.* **35** 014001
[8] Arpaia P, Ballarino A, Giunchi G and Montenero G 2014 *J. Instrum.* **9** P04020
[9] Bergen A A, van Weers H J, Bruineman C, Dhallé M M J, Krooshoop H J G, ter Brake H J M, Ravensberg K K, Jackson B D and Wafelbakker C K 2016 *Rev. Sci. Instrum.* **87** 105109
[10] Barna D 2017 *Phys. Rev. Accel. Beams* **20** 041002
[11] Capobianco-Hogan K, Cervantes R, Deshpande A, Feege N, Krahulik T, LaBounty J, Sekelsky R, Adhyatman A, Arrowsmith-Kron G, Coe B, Dehmelt K, Hemmick T, Jeffas S, LaByer T, Mahmud S, Oliveira A, Quadri A, Sharma K and Tishelman-Charny A 2018 *Nucl. Instrum. Methods Phys. Res. A* **877** 149–156
[12] Statera M, Balossino I, Barion L, Ciullo G, Contalbrigo M, Lenisa P, Lowry M, Sandorfi A and Tagliente G 2018 *Nucl. Instrum. Methods Phys. Res. A* **882** 17–21
[13] Barna D, Borburgh J, Atanasov M, Kirby G, Giunchi G, Kárpáti V, Szűcs M, Szabó G and Mertinger V 2022 *IEEE Trans. Appl. Supercond.* **32** 4000505
[14] Jiles D 2015 *Introduction to Magnetism and Magnetic Materials* 3rd ed (CRC Press)
[15] Vant-Hull L L and Mercereau J E 1963 *Rev. Sci. Instrum.* **20** 418
[16] Claycomb J R and Miller J H J 1999 *Rev. Sci. Instrum.* **70** 4562–4568
[17] Pavese F 1998 Magnetic shielding *Handbook of Applied Superconductivity* ed Bristol: Institute of Physics Publishing pp 1461–83
[18] Wu Y, Zhang G, Wu Y, Zhang D and Jing L 2023 *IEEE Trans. Appl. Supercond.* **33** 8800205
[19] Rabbers J J, Oomen M P, Bassani E, Ripamonti G and Giunchi G 2010 *Supercond. Sci. Technol.* **23** 125003
[20] Gozzelino L, Gerbaldo R, Ghigo G, Torsello D, Bonino V, Truccato M, Grigoroscuta M A, Burdusel M, Aldica G V, Sandu V, Pasuk I and Badica P 2020 *Supercond. Sci. Technol.* **33** 044018
[21] Fracasso M, Gömöry F, Solovyov M, Gerbaldo R, Ghigo G, Laviano F, Napolitano A, Torsello D and Gozzelino L 2022 *Materials* **15** 667
[22] Gozzelino L, Fracasso M, Solovyov M, Gömöry F, Napolitano A, Gerbaldo R, Ghigo G, Laviano F, Torsello D, Grigoroscuta M A, Aldica G, Burdusel M and Badica P 2022 *Supercond. Sci. Technol.* **35** 044002
[23] Barna D, Giunchi G, Novák M, Brunner K, Német A, Petrone C, Atanasov M, Bajas H and Feuvrier J 2019 *IEEE Trans. Appl. Supercond.* **29** 4101310
[24] Giunchi G, Barna D, Bajas H, Brunner K, Német A and Petrone C 2018 *IEEE Trans. Appl. Supercond.* **28** 6801705
[25] Fagnard J F, Elschner S, Bock J, Dirickx M, Vanderheyden B and Vanderbemden P 2010 *Supercond. Sci. Technol.* **23** 095012
[26] Denis S, Dusoulier L, Dirickx M, Vanderbemden P, Cloots R, Ausloos M and Vanderheyden B 2007 *Supercond. Sci. and Technol.* **20** 192–201
[27] Sasaki T, Tanaka M, Morita M, Miyamoto K M K and Hashimoto M H M 1992 *Jpn. J. Appl. Phys.* **31** 1026–1032
[28] Wéra L, Fagnard J F, Namburi D K, Shi Y, Vanderheyden B and Vanderbemden P 2017 *IEEE Trans. Appl. Supercond.* **27** 6800305
[29] Yang P, Fagnard J F, Vanderbemden P and Yang W 2019 *Supercond. Sci. Technol.* **32** 115015
[30] Zhang Z, Matsumoto S, Teranishi R and Kiyoshi T 2012 *Phys. Procedia* **27** 180–183
[31] Haseyama S, Fujinaka N, Yoshizawa S and Nakane H 2001 *Physica C Supercond.* **354** 437–440
[32] Terao Y, Sekino M, Ohsaki H, Teshima H and Morita M 2011 *IEEE Trans. Appl. Supercond.* **21** 1584–1587
[33] Douine B, Male G, Lubin T, Mezani S, Leveque J and Berger K 2014 *J. Supercond. Nov. Magn.* **27** 903–907
[34] Kvitkovic J, Pamidi S and Voccio J 2009 *Supercond. Sci. Technol.* **22** 125009
[35] Kvitkovic J, Davis D, Zhang M and Pamidi S 2013 *IEEE Trans. Appl. Supercond.* **23** 8200605
[36] Kvitkovic J, Patel S, Zhang M, Zhang Z, Peetz J, Marney A and Pamidi S 2018 *IEEE Trans. Appl. Supercond.* **28** 9001705
[37] Matsumoto S, Kiyoshi T and Uchida A 2011 *IEEE Trans. Appl. Supercond.* **21** 2283–2286
[38] Kvitkovic J, Burnside K, Zhang M and Pamidi S 2020 *J. Phys.: Conf. Ser.* **1559** 012117
[39] Álvarez A, Rivera B, Pérez B and Suárez P 2023 *IEEE Access* **11** 22835–22842
[40] Solovyov M, Šouc J, Kucharovič M and Gömöry F 2021 *IEEE Trans. Appl. Supercond.* **31** 4901205
[41] Solovyov M, Šouc J, Gömöry F, Rikel M O, Mikulášová E, Ušáková M and Ušák E 2017 *IEEE Trans. Appl. Supercond.* **27** 8800204
[42] Nagasaki Y, Solovyov M and Gömöry F 2018 *IEEE Trans. Appl. Supercond.* **28** 6601905
[43] Kvitkovic J, Davis D, Zhang M and Pamidi S 2015 *IEEE Trans. Appl. Supercond.* **25** 8800304
[44] Gu C, Chen S, Pang T and Qu T M 2017 *Appl. Phys. Lett.* **110** 193505
[45] Wang S Y, Wang S S, Yu X, Xu H, Li Y Y, Jiang H Y and Sun K Y 2023 *Supercond. Sci. Technol.* **36** 035001
[46] Tomków L, Kulikov E, Kozłowski K and Drobin V 2019 *J.*

Appl. Phys. **126** 083903
[47] Bortot L, Mentink M, Petrone C, Nugteren J V, Deferne G, Koettig T, Kirby G, Pentella M, Perez J C, Pincot F O, Rijk G D, Russenschuck S, Verweij A P and Schöps S 2021 *Supercond. Sci. Technol.* **34** 105001
[48] Peng Y, Zeng Z, Zhou D, Zhao W, Jia Z, Guo Y, Bai C, Fan F, Chen Y and Cai C 2021 *J. Supercond. Nov. Magn.* **34** 2493–2501
[49] Brialmont S, Dular J, Wéra L, Fagnard J F, Vanderheyden B, Geuzaine C, Hahn S, Patel A and Vanderbemden P 2023 *Supercond. Sci. Technol.* **36** 054004
[50] Fagnard J F, Dirickx M, Levin G A, Barnes P N, Vanderheyden B and Vanderbemden P 2010 *J. Appl. Phys.* **108** 013910
[51] Wéra L, Fagnard J F, Levin G A, Vanderheyden B and Vanderbemden P 2015 *Supercond. Sci. Technol.* **28** 074001
[52] Chi C, Cai C, Zhou D, Guo Y, Yan W, Bai C, Liu Z, Lu Y, Fan F, Li M and Zeng Z 2020 *Supercond. Sci. Technol.* **33** 095001
[53] Tomków L, Ciszek M and Chorowski M 2015 *J. Appl. Phys.* **117** 043901
[54] Motoki T, Yanai Y, Nunokawa K and Shimoyama J 2020 *Appl. Phys. Express* **13** 093002
[55] Motoki T, Sasada R, Tomihisa T, Miwa M, Nakamura S and Shimoyama J 2022 *Supercond. Sci. Technol.* **35** 094003
[56] Antončík F, Lojka M, Hlásek T, Sedmidubský D, Baumann J, Durrell J H, Cardwell D A and Jankovský O 2023 *J. Am. Ceram. Soc.* 1–11
[57] Levin G A, Barnes P N, Murphy J, Brunke L, Long J D, Horwath J and Turgut Z 2008 *Appl. Phys. Lett.* **93** 062504
[58] Lee H G, Kim J G, Lee S W, Kim W S, Lee S W, Choi K D, Hong G W and Ko T K 2006 *Phys. C: Supercond. Appl.* **445-448** 1099–1102
[59] Sheng J, Zhang M, Wang Y, Li X, Patel J and Yuan W 2017 *Supercond. Sci. Technol.* **30** 094002
[60] Zheng Y, Wang Y, Li J and Jin Z 2017 *AIP Adv.* **7** 095218
[61] Ali M Z, Zheng J, Huber F, Zhang Z, Yuan W and Zhang M 2020 *Supercond. Sci. Technol.* **33** 04LT01
[62] Zhao C, Shi J, Sheng J and Chen W 2022 *Crystals* **12** 1438
[63] Rotheudt N, Fagnard J F, Harmeling P and Vanderbemden P 2023 *Cryogenics* **133** 103693

Appendix A. Additional results

This appendix shows the results for the configurations that are not described in section 3. In Figure A1, all the configurations using the hollow bulk (HB) are compared in terms of the spatial distribution of SF along y, for $z = 5.7$ mm, similarly to Figure 5. The observations are perfectly in line with those related to the full disk-shaped bulk (section 3). First, using hybrid configurations allows us to reach higher SF over larger surfaces. Then, the larger the loops, the smaller the maximum SF. Combining both sizes of loops allows us to reach a globally higher SF. Finally, the spatial extension of the region SF > 2 for $y < 0$ is greater for larger loops, yielding a trade-off in the choice of the size of the closed-loop coated conductors.

Figure A2 compares the spatial distribution of SF, for $z = 5.7$ mm, for three configurations using only closed-loop coated conductors. The observations are fully consistent with those mentioned in section 3 and

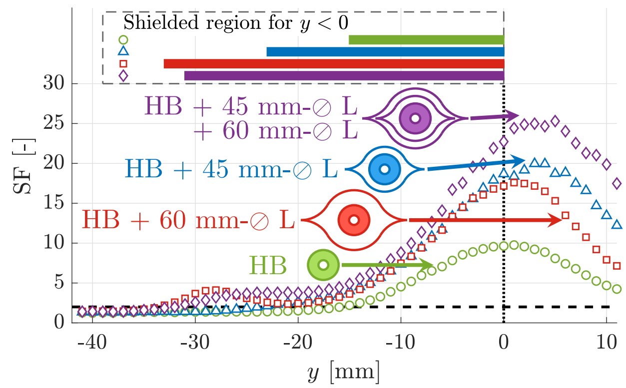

Figure A1. Spatial distribution of SF along y, for $z = 5.7$ mm. The open green circles ○ show the SF when the hollow bulk is used alone. The open blue triangles △ are related to the hollow bulk combined with 45 mm-diameter closed-loop coated conductors. The open red squares □ are for the bulk combined with the 60 mm-diameter loops. The open violet diamonds ◇ correspond to the bulk with 45 mm-diameter loops and 60 mm-diameter loops. The dotted black line indicates the central position $y = 0$. The rectangles at the top of the graph indicate in each of the three cases the spatial extension of the region SF > 2 for $y < 0$. The limit SF $= 2$ is shown by a dashed black line.

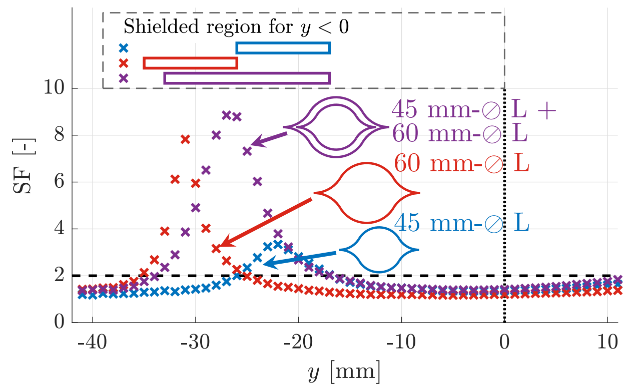

Figure A2. Spatial distribution of SF along y, for $z = 5.7$ mm. The blue crosses × show the SF when the 45 mm-diameter closed-loop coated conductors are used alone. The red crosses × are for the 60 mm-diameter loops alone. The violet crosses × correspond to the 45 mm-diameter loops and the 60 mm-diameter loops together. The dotted black line indicates the central position $y = 0$. The rectangles at the top of the graph indicate in each of the three cases the spatial extension of the region SF > 2 for $y < 0$. The limit SF $= 2$ is shown by a dashed black line.

section 4. Such relatively large loops provide a very limited screening effect around the central position, as SF < 1.5 in the three cases. The only region for which a noticeable screening effect is observed is above the superconductor, i.e., around $|y| = D/2$, where D is the diameter of the considered closed-loop coated conductors.